MRI Assessment of Neuropathology in a Transgenic Mouse Model of Alzheimer's Disease

Joseph A. Helpern,[1–4*] Sang-Pil Lee,[1] Maria F. Falangola,[1,3] Victor V. Dyakin,[1] Adam Bogart,[1] Babak Ardekani,[1,2] Karen Duff,[1,2] Craig Branch,[1,5,6] Thomas Wisniewski,[1,7] Mony J. de Leon,[1,2] Oliver Wolf,[8] Jacqueline O'Shea,[1] and Ralph A. Nixon[1,2,9]

The cerebral deposition of amyloid β-peptide, a central event in Alzheimer's disease (AD) pathogenesis, begins several years before the onset of clinical symptoms. Noninvasive detection of AD pathology at this initial stage would facilitate intervention and enhance treatment success. In this study, high-field MRI was used to detect changes in regional brain MR relaxation times in three types of mice: 1) transgenic mice (PS/APP) carrying both mutant genes for amyloid precursor protein (APP) and presenilin (PS), which have high levels and clear accumulation of β-amyloid in several brain regions, starting from 10 weeks of age; 2) transgenic mice (PS) carrying only a mutant gene for presenilin (PS), which show subtly elevated levels of Aβ-peptide without β-amyloid deposition; and 3) nontransgenic (NTg) littermates as controls. The transverse relaxation time T_2, an intrinsic MR parameter thought to reflect impaired cell physiology, was significantly reduced in the hippocampus, cingulate, and retrosplenial cortex, but not the corpus callosum, of PS-APP mice compared to NTg. No differences in T_1 values or proton density were detected between any groups of mice. These results indicate that T_2 may be a sensitive marker of abnormalities in this transgenic mouse model of AD. Magn Reson Med 51:794–798, 2004. © 2004 Wiley-Liss, Inc.

Key words: MRI; transgenic mice; Alzheimer's disease; β-amyloid

Cerebral deposits of the amyloid β-peptide and alterations of neurophysiology develop some years before Alzheimer's disease can be diagnosed clinically (1–3). By this stage, brain pathology is extensive and includes irreversible loss of neurons in brain regions essential for normal cognition (3). Because AD therapy is likely to be most successful when intervention occurs before neurons are irreversibly damaged or lost, noninvasive methods to detect early yet subtle changes in the brain would have considerable clinical value. Currently, there are no sensitive and specific biological markers for the preclinical stages of AD.

Recent MRI studies of humans with mild cognitive impairment have shown that brain volume losses associated with neurodegeneration in the hippocampus have value in predicting increased risk for developing AD (4,5). Moreover, advances in high field strength MRI technology now raise the possibility that more subtle alterations of morphology or physiology preceding neurodegeneration might be detectable, including, in the case of AD, early effects of β-amyloid deposition. Since intrinsic MR parameters, such as transverse (T_2) and longitudinal (T_1) relaxation times are sensitive to changes in the biophysical environment of water, we hypothesized that the presence of increased deposition of β-amyloid in the brain would have an effect on these parameters.

To investigate the possibility of early detection of the pathophysiology associated with AD, we studied PS/APP and PS transgenic mice together with nontransgenic (NTg) controls with MRI at 7 T. PS transgenic mice carry only a mutant gene for presenilin-1 (PS), which show subtly elevated levels of Aβ-peptide without β-amyloid deposition in the brain (6). PS/APP transgenic mice express the human genes for amyloid precursor protein (APP) and presenilin-1 (PS) (7), which harbor mutations, $APP_{K670N,M671L}$ and PS_{M146V}, known to cause familial AD (FAD) in humans. In these mice, β-amyloid begins to deposit at 10–12 weeks of age and progressively accumulates as plaque-like lesions throughout their life span, reaching levels exceeding those in AD brain. Several other features of the human disease are also seen, including dystrophy of some neurites and mild local inflammation within the plaques (8); however, neurofibrillary tangle formation is absent and neuronal cell loss has not been detected by stereological analysis (9). These mice, therefore, represent a model of extensive β-amyloidosis with a level of tissue injury corresponding most closely to the early stages of AD.

In this study, we acquired quantitative parametric maps of transverse (T_2) and longitudinal (T_1) relaxation times, along with proton density, to help characterize the biophysical environment of water as an independent measure of altered cellular physiology. Our results validate MRI as

[1]Nathan S. Kline Institute, Orangeburg, New York.

[2]Department of Psychiatry, New York University School of Medicine, New York, New York.

[3]Department of Radiology, New York University School of Medicine, New York, New York.

[4]Department of Physiology and Neuroscience, New York University School of Medicine, New York, New York.

[5]Department of Radiology, Albert Einstein College of Medicine, Bronx, New York.

[6]Department of Neuroscience, Albert Einstein College of Medicine, Bronx, New York.

[7]Department of Neurology, New York University School of Medicine, New York, New York.

[8]University of Duesseldorf, Duesseldorf, Germany

[9]Department of Cell Biology, New York University School of Medicine, New York, New York.
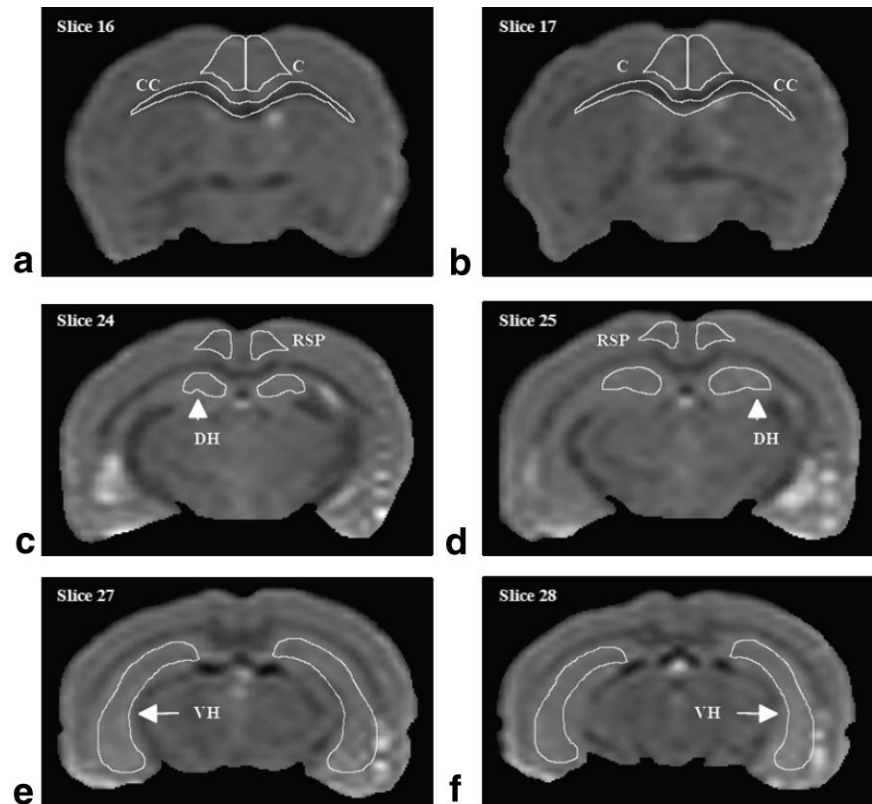
FIG. 1. ROIs used for T_1 and T_2 analysis. Six representative MRI transverse slices showing examples of ROIs used: cingulate cortex (C) and corpus callosum (CC) (slices 16 and 17); retrosplenial cortex (RSP) and dorsal hippocampus (DH) (slices 24 and 25); ventral hippocampus (VH) (slices 27 and 28).

a sensitive tool to identify regional differences in the brains of a transgenic mouse model of Alzheimer's disease that may be associated with Aβ-peptide deposition.

MATERIALS AND METHODS

Transgenic Mice

Transgenic mice expressing mutant human APP$_{K670N,M671L}$ protein (line Tg2576) (10) and a line of mice expressing human mutant PS1$_{M146V}$ protein (line 8.9) (6) were crossed to generate offspring including parental type singly transgenic (APP and PS1) offspring, doubly transgenic PS/APP animals, and nontransgenic littermates (8). Nine mice for each genotype (16–23 months of age) were studied.

MRI Protocols

MRI was performed using a 7 T 40-cm bore magnet equipped with a 10-cm gradient insert capable of 1000 mT/m in 400 μs (Magnex Scientific, Abingdon, UK) interfaced to an SMIS console (SMIS, Guilford, UK). Mice were initially anesthetized with isoflurane (2%) in NO$_2$ (75%) and O$_2$ (25%) and maintained with 1% of isoflurane during MR experiments using a facemask. Core body temperature was kept to 37°C using a temperature-controlled water blanket. Animals were placed in a 20 mm birdcage RF coil with a home-built mouse head holder. For T_2 measurements, a multislice spin-echo sequence was used. Imaging parameters were: one signal average, 48 slices, FOV 2.56 × 2.56 cm^2, matrix size 128 × 96, echo times (TE) of 15, 20, 25, 35, 55, and 75 ms, and repetition time

(TR) of 4000 ms. For T_1 measurements, an inversion prepared, segmented TurboFlash sequence based on the PURR sequence (progressively unsaturated relaxation during perturbed recovery from inversion) (11) with 64 linear time increments, 16 segments, 4 signal averages, a TR of 10 sec, a TE of 5 ms, and the same FOV and matrix as above. We also acquired high-resolution (53 × 72 μm in-plane and 200 μm slice thickness) T_2-weighted images of fixed PS/APP and PS mouse brains using a fast spin echo sequence. Image acquisition parameters were: FOV 13.8 × 13.8 mm^2, matrix 256 × 192, TE/TR 10/6000 ms, 128 signal average, and an echo train length of 4.

Estimation of T_1 and T_2

For the calculation of T_2, regions of interest (ROIs) were manually drawn on two consecutive slices using the STIMULATE program (12). ROIs were placed at the level of the dorsal and ventral portions of the hippocampus, cortex (cingulate and retrosplenial), and corpus callosum (Fig. 1). An ROI in the muscle was used as an internal control. In order to estimate T_2 relaxation times for each ROI, a mean image intensity value was computed at different TEs and fitted to a single exponential curve with two parameters.

T_1 and proton density were calculated from ROIs drawn on a single slice covering the dorsal portion of the hippocampus, cingulate cortex, and temporal muscle. The mean signal intensities in the given ROI were fitted to a single exponential function after subtracting the image with the longest inversion time in phase sensitive fashion (13). Proton density was calculated by normalizing image

Table 1
Comparison of Regional Brain T_2 Values[a] in Transgenic Mice

	Hippocampus[b]	Cingulate	Retrosplenial cortex	Corpus callosum	Muscle
PS/APP	39.31	37.01	35.45	34.60	24.12
	(2.96)	(2.87)	(3.13)	(2.16)	(1.25)
PS	40.79	38.83	37.22	35.21	24.05
	(2.12)	(1.91)	(2.21)	(2.23)	(1.00)
NTg	42.45	40.13	38.74	35.63	23.71
	(1.85)	(1.32)	(3.37)	(0.78)	(1.00)
P-value PS/APP vs. NTg	0.016[c]	0.009[c]	0.047[c]	0.198	0.457
P-value PS/APP vs. PS	0.242	0.132	0.272	0.564	0.902
P-value PS vs. NTg	0.094	0.114	0.272	0.535	0.481

[a]All T_2 values are given in ms units as mean ($\pm$SD).
[b]Hippocampus ROI consisted of two slices from dorsal region and two slices from ventral region.
[c]Statistically significant difference was assigned for $P < 0.05$.

intensity of hippocampus and cingulated cortex with that of muscle.

Statistical Analysis

Means and standard deviations for T_2, T_1, and proton density for each ROI were calculated. Mean values were compared using Student's *t*-test assuming equal variance. Statistical significance was assigned for $P < 0.05$.

RESULTS

Table 1 shows the T_2 values of various brain regions consisting of the hippocampus, cingulate cortex, retrosplenial cortex, corpus callosum, and muscle. When compared to age-matched nontransgenic (NTg) controls, PS/APP mice showed significantly reduced T_2 values in the cingulate ($P = 0.009$) and retrosplenial cortex ($P = 0.047$), and hippocampus ($P = 0.016$). No significant differences in T_2 values were evident in the corpus callosum for NTg and PS/APP or in any brain region between PS and PS/APP or PS and NTg groups. Muscle, used as an internal control, demonstrated no differences among all three genotypes, indicating reliability of the T_2 measurements. No significant differences in T_1 relaxation times or proton density were found between the three genotypes.

Shown in Fig. 2 are representative high-resolution MR images from PS and PS/APP fixed brain. Examples of Aβ immunolabeled histological images from different, but representative, PS and PS/APP mice are shown in Fig. 3. The PS/APP histological section shows extensive amyloid deposition, while the PS histological section is void of amyloid deposition. A similar difference was observed for the presence and absence of signal hypointensities in the high-resolution MRI of PS/APP and PS mouse brains, respectively.

DISCUSSION

Proton density and T_1 values did not show any significant differences in the three genotypes. This is not necessarily surprising, since both T_1 and proton density are generally less sensitive to pathophysiology. The regional T_2 changes shown here in the hippocampus and cingulate and retrosplenial cortices imply alterations of cell physiology in the

PS/APP mice. These regions are consistent with a previous report (14) of PS/APP mice having greater levels of amyloid deposition associated with astrocytosis in the cortex and hippocampus. Also, the highest transgene expression is present in the cortex and the CA3 region of the hippocampus (8). Since there was no significant T_2 difference between PS/APP and PS or PS and NTg, the overexpression of APP may be the predominant factor associated with the shortening of T_2 in PS/APP mice. Although the T_2 values of PS mice are not statistically different from other genotypes, the T_2 values were shorter than those of NTg, but longer than PS/APP mice. Although this trend suggests a possible influence of PS gene expression on T_2 values, the explicit effect of gene expression on T_2 remains unknown.

It is possible that the reductions in T_2 demonstrated here might be the result of reduced cerebral blood flow (CBF). Reductions of T_2 have been associated with reduced CBF in rats (15), which was attributed to decreased blood oxygenation in areas of diminished perfusion. In this study, T_2 reductions of 6% were associated with CBF reductions from 15–60% (15). Recently, Niwa et al. (16) demonstrated a 40–46% reduction of CBF and a 30–40% reduction of cerebral glucose utilization in similar transgenic mouse models of β-amyloid overproduction, compared with age-matched, nontransgenic littermates. Considering the high loads of β-amyloid in the parenchyma and cerebral vasculature of the PS/APP mice used in our study (17), a reduction of CBF would not be surprising and indeed might contribute to the 6–8% average reduction in T_2 observed. Interestingly, the corpus callosum, which is the only white matter region studied, did not show a significant reduction in T_2. Since white matter baseline CBF is known to be 3–4 times less than gray matter, it might be expected that white matter T_2 would be less affected by changes in CBF.

In order to further investigate possible sources of T_2 reduction in PS/APP mice, we acquired high-resolution T_2-weighted images of PS and PS/APP fixed mouse brain (Fig. 2). The most striking observation is the presence of numerous signal hypointensities in the MR images of PS/APP mice and the absence of any similar pattern of signal hypointensities in the PS mice. This is remarkably consistent with the histological pattern of distribution of plaque deposition described in the literature (7,14), and illus-

FIG. 2. Ultrahigh-resolution MR images of 18-month-old transgenic mouse brain. Two representative MR images of fixed transgenic mouse brains obtained without contrast reagents. Numerous signal hypointensities are apparent in the cortex of the PS/APP mouse brain (**a**), whereas no similar pattern of signal hypointensities is apparent in the PS mouse brain (**b**).
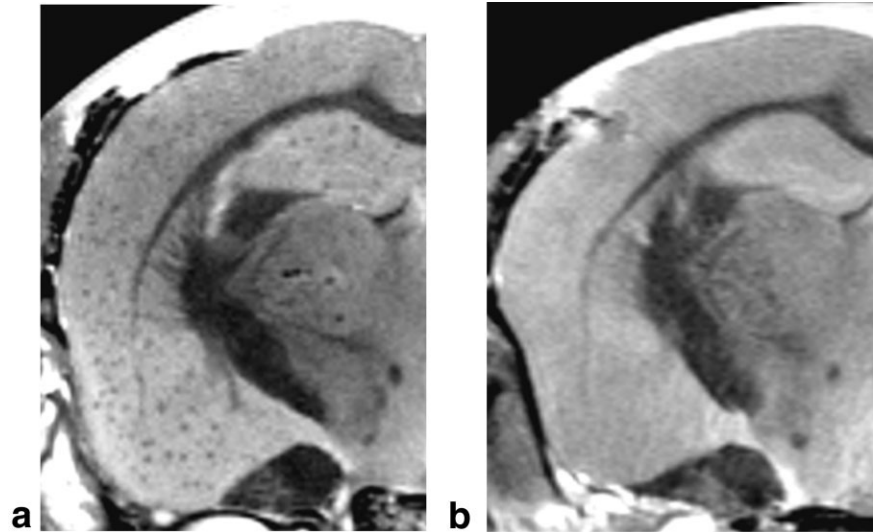
trated here with two β-amyloid-immunostained histological images from different PS and PS/APP mice (Fig. 3). Although the T_2-weighted images presented here are not quantitative in nature, the similarity in the general pattern of distribution of histologically defined plaques and MRI signal hypointensities is intriguing and may suggest an influence of plaque on T_2 reductions as measured in the ROI analysis. Further quantitative work will be necessary in order to determine the explicit influence of plaques in T_2.

Reduced T_2 in human AD has been associated with iron deposition in basal ganglia (18). Although the association of iron and plaques in PS/APP mice is not known, iron has been associated with plaque in similar transgenic mouse models (19). Therefore, the reason for the reduction in T_2 shown in the current study cannot exclude the possibility of a contribution from elevated iron levels in the plaque of PS/APP mice. Indeed, the accumulation of iron in these plaques could be responsible for the hypointensities observed in our high-resolution images.

Finally, cell shrinkage has been associated with decreased T_2 (20) and it is of interest to note that cell size is regulated by the lysosomal system (21), which is markedly activated in AD and also upregulated in PS/APP mice (22). Evidence of this may be elucidated by MR diffusion studies, which we are in the process of performing.

Our data demonstrate that quantitative measurements of T_2 can provide evidence of early involvement of regional pathophysiological changes in the absence of neuronal cell loss in mouse brains exhibiting amyloid plaque neuropathology. The demonstration here of disease-relevant functional abnormalities before appreciable numbers of neurons are lost underscores the promise of MRI as an aid to the early diagnosis of AD and assessment of treatment efficacy.

ACKNOWLEDGMENT
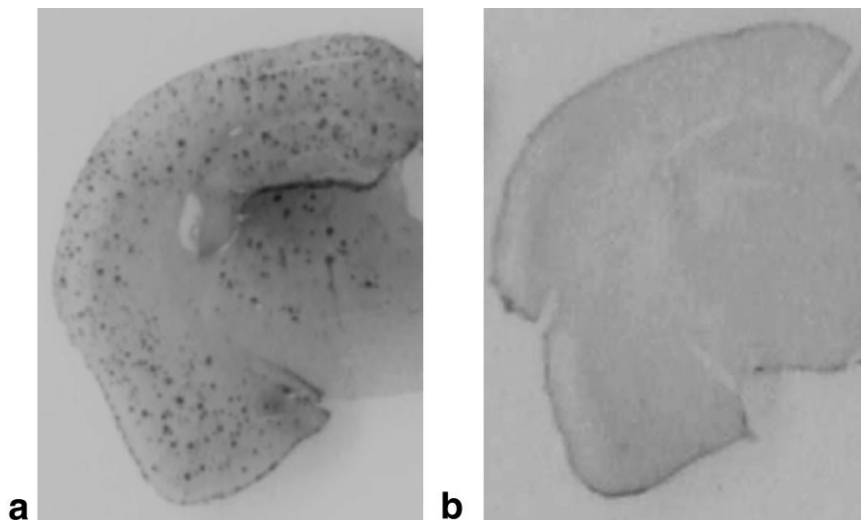
FIG. 3. Histological images of 18-month-old transgenic mouse brain. Aβ immunolabeled histological images representative of the pattern of distribution of plaque deposition described in the literature for a PS/APP mouse (**a**) and the absence of plaques in a PS mouse (**b**). To visualize the Aβ plaques, immunohistochemistry was performed using antibody 6E10 at 1:1000 from Sigma (St. Louis, MO). Sections were immunostained by a standard avidin-biotin complex method using diaminobenzidine as chromogen.

REFERENCES

1. Morris JC, Storandt M, McKeel DW Jr, Rubin EH, Price JL, Grant EA, Berg L. Cerebral amyloid deposition and diffuse plaques in "normal" aging: evidence for presymptomatic and very mild Alzheimer's disease. Neurology 1996;46:707−719.

2. Cataldo A, Peterhoff C, Troncoso J, Gomez-Isla T, Hyman B, Nixon R. Endocytic pathway abnormalities precede beta-amyloid deposition in sporadic Alzheimer's disease: differential effects of APOE genotype and presenilin mutations. Am J Pathol 2000;157:277−286.

3. Haroutunian V, Perl DP, Purohit DP, Marin D, Khan K, Lantz M, Davis KL, Mohs RC. Regional distribution of neuritic plaques in the nondemented elderly and subjects with very mild Alzheimer disease [see Comments]. Arch Neurol 1998;55:1185−1191.

4. de Leon MJ, Golomb J, George AE, Convit A, Tarshish CY, McRae T, De Santi S, Smith G, Ferris SH, Noz M. The radiologic prediction of Alzheimer disease: the atrophic hippocampal formation. AJNR Am J Neuroradiol 1993;14:897−906.

5. Xu Y, Jack CR Jr, O'Brien PC, Kokmen E, Smith GE, Ivnik RJ, Boeve BF, Tangalos RG, Petersen RC. Usefulness of MRI measures of entorhinal cortex versus hippocampus in AD. Neurology 2000;54:1760−1767.

6. Duff K, Eckman C, Zehr C, Yu X, Prada CM, Perez-tur J, Hutton M, Buee L, Harigaya Y, Yager D, Morgan D, Gordon MN, Holcomb L, Refolo L, Zenk B, Hardy J, Younkin S. Increased amyloid-beta42(43) in brains of mice expressing mutant presenilin 1. Nature 1996;383:710−713.

7. Holcomb L, Gordon MN, McGowan E, Yu X, Benkovic S, Jantzen P, Wright K, Saad I, Mueller R, Morgan D, Sanders S, Zehr C, O'Campo K, Hardy J, Prada CM, Eckman C, Younkin S, Hsiao K, Duff K. Accelerated Alzheimer-type phenotype in transgenic mice carrying both mutant amyloid precursor protein and presenilin 1 transgenes. Nat Med 1998; 4:97−100.

8. McGowan E, Sanders S, Iwatsubo T, Takeuchi A, Saido T, Zehr C, Yu X, Uljon S, Wang R, Mann D, Dickson D, Duff K. Amyloid phenotype characterization of transgenic mice overexpressing both mutant amyloid precursor protein and mutant presenilin 1 transgenes. Neurobiol Dis 1999;6:231−244.

9. Takeuchi A, Irizarry MC, Duff K, Saido TC, Hsiao Ashe K, Hasegawa M, Mann DM, Hyman BT, Iwatsubo T. Age-related amyloid beta deposition in transgenic mice overexpressing both Alzheimer mutant presenilin 1 and amyloid beta precursor protein Swedish mutant is not associated with global neuronal loss. Am J Pathol 2000;157:331−339.

10. Hsiao K, Chapman P, Nilsen S, Eckman C, Harigaya Y, Younkin S, Yang F, Cole G. Correlative memory deficits, Abeta elevation, and amyloid plaques in transgenic mice [see Comments]. Science 1996;274:99−102.

11. Labadie C, Lee JH, Vetek G, Springer CS Jr. Relaxographic imaging. J Magn Reson B 1994;105:99−112.

12. Strupp JP. Stimulate: a GUI based fMRI analysis software package. NeuroImage 1996;3:S607.

13. Kim S-G, Hu X, Ugurbil K. Accurate T_1 determination from inversion recovery images: application to human brain at 4 T. Magn Reson Med 1994;31:445−449.

14. Wengenack TM, Whelan S, Curran GL, Duff KE, Poduslo JF. Quantitative histological analysis of amyloid deposition in Alzheimer's double transgenic mouse brain. Neuroscience 2000;101:939−944.

15. Grohn OH, Kettunen MI, Penttonen M, Oja JM, van Zijl PC, Kauppinen RA. Graded reduction of cerebral blood flow in rat as detected by the nuclear magnetic resonance relaxation time T2: a theoretical and experimental approach. J Cereb Blood Flow Metab 2000;20:316−326.

16. Niwa K, Kazama K, Younkin SG, Carlson GA, Iadecola C. Alterations in cerebral blood flow and glucose utilization in mice overexpressing the amyloid precursor protein. Neurobiol Dis 2002;9:61−68.

17. Kurt MA, Davies DC, Kidd M, Duff K, Rolph SC, Jennings KH, Howlett DR. Neurodegenerative changes associated with beta-amyloid deposition in the brains of mice carrying mutant amyloid precursor protein and mutant presenilin-1 transgenes. Exp Neurol 2001;171:59−71.

18. Bartzokis G, Sultzer D, Cummings J, Holt LE, Hance DB, Henderson VW, Mintz J. In vivo evaluation of brain iron in Alzheimer disease using magnetic resonance imaging. Arch Gen Psychiatry 2000;57:47−53.

19. Smith MA, Harris PL, Sayre LM, Perry G. Iron accumulation in Alzheimer disease is a source of redox-generated free radicals. Proc Natl Acad Sci USA 1997;94:9866−9868.

20. O'Shea JM, Williams SR, van Bruggen N, Gardner-Medwin AR. Apparent diffusion coefficient and MR relaxation during osmotic manipulation in isolated turtle cerebellum. Magn Reson Med 2000;44:427−432.

21. Cataldo AM, Hamilton DJ, Barnett JL, Paskevich PA, Nixon RA. Properties of the endosomal-lysosomal system in the human central nervous system: disturbances mark most neurons in populations at risk to degenerate in Alzheimer's disease. J Neurosci 1996;16:186−199.

22. Nixon R, Mathews P, Cataldo A, Mohan P, Schmidt S, Duff K, Berg M, Marks N, Peterhoff C, Sershen H. In vivo perturbation of lysosomal function promotes neurodegeneration in the PS1M146V/APPK670N,M671L mouse model of Alzheimer's disease pathology, In: Iqbal K, Sisodia S, Winblad B, editors. Alzheimer's disease: advances in etiology, pathogenesis and therapeutics. London: John Wiley & Sons; 2001.